Arctic Sea Ice Loss and Eurasian Cooling in Winter 2020-21

Nishii, Kazuaki
Graduate School of Bioresouces, Mie University

Taguchi, Bunmei
Faculty of Sustainable Design, University of Toyama

Mori, Masato
Research Institute for Applied Mechanics, Kyushu University

Kosaka, Yu
Research Center for Advanced Science and Technology, The University of Tokyo

他

出版情報：SOLA. 18, pp.199-204, 2022. Meteorological Society of Japan
バージョン：
権利関係：©The Author(s)

Arctic Sea Ice Loss and Eurasian Cooling in Winter 2020−21

Kazuaki Nishii[1], Bunmei Taguchi[2], Masato Mori[3], Yu Kosaka[4], and Hisashi Nakamura[4]
[1]*Graduate School of Bioresouces, Mie University, Tsu, Japan*
[2]*Faculty of Sustainable Design, University of Toyama, Toyama, Japan*
[3]*Research Institute for Applied Mechanics, Kyushu University, Kasuga, Japan*
[4]*Research Center for Advanced Science and Technology, The University of Tokyo, Tokyo, Japan*

Abstract

Anomalous coldness was observed over midlatitude Eurasia in December 2020 and over subpolar Eurasia in January 2021. The former was accompanied by the Warm Arctic and Cold Eurasia (WACE) pattern, while the latter by the negative phase of the Arctic Oscillation (AO). A set of large ensemble experiments with an atmospheric general circulation model suggests a contribution of reduced Arctic Sea ice to the midlatitude cooling and WACE pattern in December 2020. The tropical and extratropical sea surface temperature (SST) anomalies, however, contribute to warming over midlatitude Eurasia. In January 2021, neither the sea ice nor SST anomalies can explain the subpolar Eurasian cooling and the negative AO in our experiments.

(**Citation**: Nishii, K., B. Taguchi, M. Mori, Y. Kosaka, and H. Nakamura, 2022: Arctic Sea ice loss and Eurasian cooling in winter 2020−21. *SOLA*, **18A**, 199−204, doi:10.2151/sola.2022-032.)

1. Introduction

In the early 2020−21 winter, China experienced several outbreaks of extreme cold waves that accompany blockings over Eurasia (e.g., Bueh et al. 2022). Impacts of the sea ice anomaly (SIA) in the Arctic, La Niña, and warm sea surface temperature anomalies (SSTAs) in the North Atlantic on those cold waves have been discussed (Yao et al. 2022; Zhang et al. 2022; Zheng et al. 2022). Among them, Zhang et al. (2022; hereafter referred to as ZZD22) argued through atmospheric general circulation model (AGCM) experiments that the SIA and warm SSTA in the extratropical North Pacific associated with the Pacific decadal oscillation (PDO) have potential to induce those cold waves.

The impact of the SIAs in Arctic on midlatitude weather, however, has been under intense debate (e.g., Overland et al. 2021). Some studies argued that SIA in the Barents-Kara Seas (BKS) can induce the Warm Arctic and Cold Eurasia (WACE) pattern that accompanies warming over the Arctic and cooling over midlatitude Eurasia (Inoue et al. 2012; Mori et al. 2014, 2019), while others argued that atmospheric blocking over the Ural Mountains can force the WACE pattern and SIA, and thus cause their covariation and interaction (e.g., Tyrlis et al. 2019). Some studies argue that the SIA impact on Eurasian temperatures is indiscernible in AGCMs and seasonal forecast models (e.g., Ogawa et al. 2018; Komatsu et al. 2022).

The aim of this study is to evaluate the impact of the SIA and SSTA on the 2020−21 winter climate in Eurasia, based on large ensemble experiments of an AGCM. Our AGCM is independent from that used in ZZD22. We also investigate whether concurrent SIA and SSTA could trigger the WACE pattern. In addition, we discuss the Arctic Oscillation (AO; Thompson and Wallace 1998) and associated surface air temperature (SAT) variability in subpolar Eurasia (Mori et al. 2014; Nakamura et al. 2015).

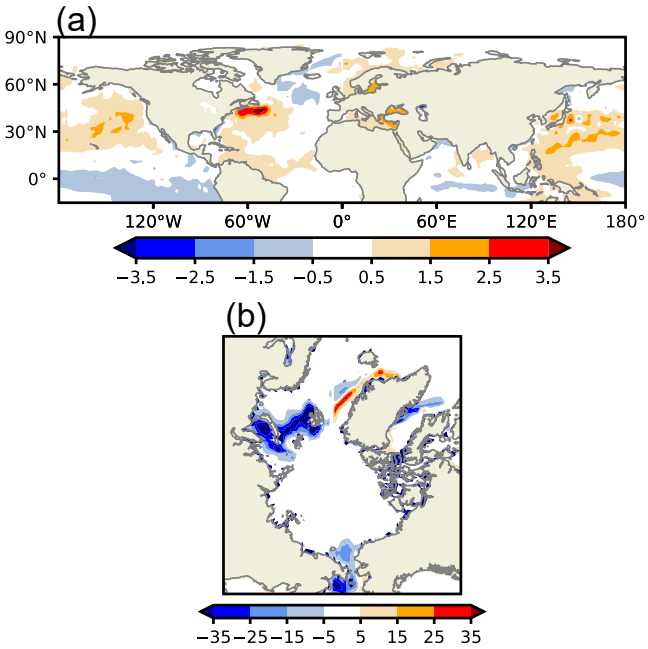

Fig. 1. (a) Observed SSTAs averaged in December 2020 and January 2021. The unit is K. (b) As in (a), but for SIAs (%).

2. Data and method

2.1 Data

We use the Japanese 55-year Reanalysis (JRA-55) dataset (Kobayashi et al. 2015). Daily SST and sea ice concentration (SIC) data prescribed to our AGCM were taken from the US National Oceanic and Atmospheric Administration (NOAA) Optimally Interpolated Advanced Very High Resolution Radiometer Pathfinder SST (OISST) data compiled on a 0.25° × 0.25° grid. Its version 2.1 (Huang et al. 2021) is used for the 2020−21 winter, while its version 2 (Reynolds et al. 2007) is adopted for the daily climatological seasonal cycles defined as their local averages between 1982 and 2013 for individual calendar days.

The observed SSTA and SIA averaged over December 2020 and January 2021 are shown in Fig. 1. In the tropical Pacific, a moderate cool SSTA was observed around the dateline, while warm SSTAs in the midlatitude North Pacific and Atlantic exceed three standard deviations. The SICs are lower than its climatology over the BKS and Bering Strait. In particular, the SIC averaged over BKS (70°N−80°N, 30°E−80°E) is the 3rd smallest in the last 40 seasons (from 1981−82 to 2020−21).

2.2 Numerical simulations

We used an AGCM for the Earth Simulator (AFES; Ohfuchi et al. 2004; Kuwano-Yoshida et al. 2010). The horizontal resolution is T119 (about 100 km) and the model top is around the 0.1-hPa pressure level. We performed five sets of AGCM experiments

Corresponding author: Kazuaki Nishii, Graduate School of Bioresources, Mie University, 1577 Kurimamachiya-cho, Tsu, Mie 514-8507, Japan. E-mail: nishii@bio.mie-u.ac.jp.

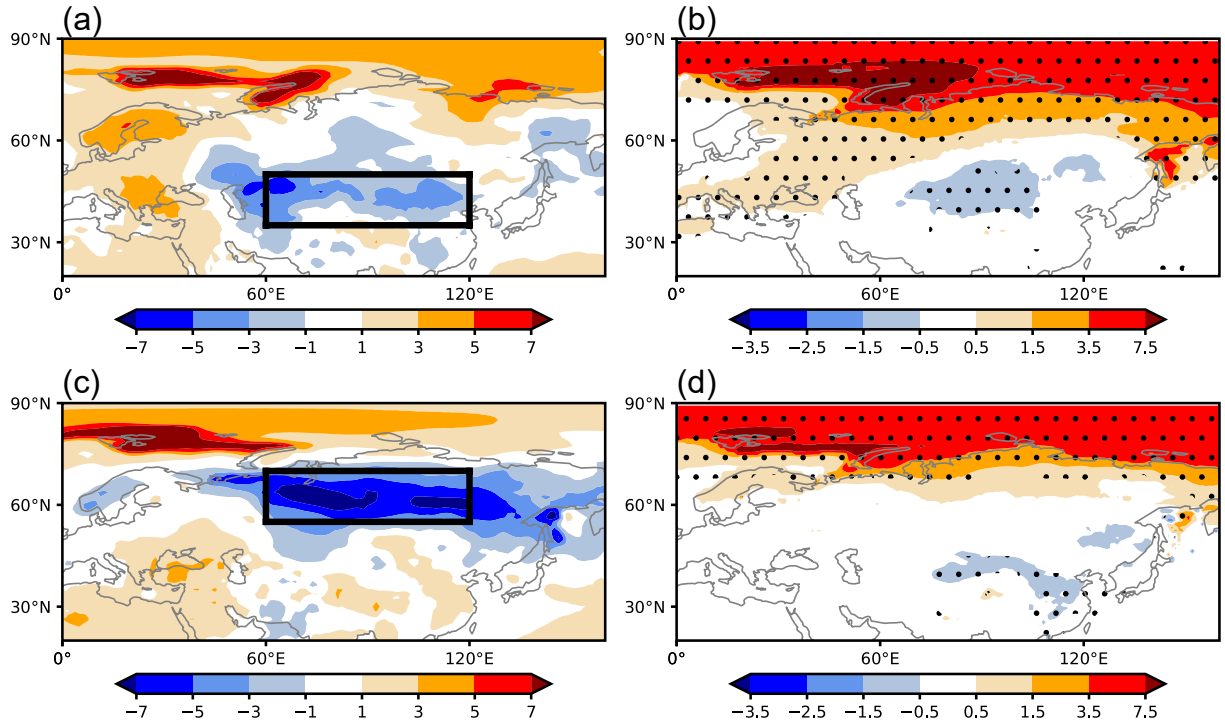

Fig. 2. (a) SATAs in December 2020 based on JRA-55. The unit is K. (b) As in (a), but for AGCM response in SAT to observed SIAs. Dots represent anomalies significant at the 5% level with Student's *t*-test. (c) As in (a), but for January 2021. (d) As in (b), but for January 2021. Black squares in (a) and (b) represent domains for the midlatitude Eurasia (35°N−50°N, 60°E−120°E) and subpolar Eurasia (55°N−70°N, 60°E−120°E).

Table 1. Simulated ensemble-mean responses of SAT over mid-latitude Eurasia, the WACE index, SAT over subpolar Eurasia, and the AO index to observed anomalies of sea ice, global SST, tropical SST, extratropical SST, and sea ice and global SST. See Supplement 1 for the definition of responses. SATAs and indices in JRA-55 are also shown. Asterisks indicate responses statistically significant at the 5% level with Student's *t*-test.

	December 2020		January 2021	
	Midlatitude Eurasia SAT (K)	The WACE index	Subpolar Eurasia SAT (K)	The AO index
Sea ice	−0.4*	1.7*	0.5	0.1
Global SST	1.0*	0.4*	2.3*	0.2*
Tropical SST	0.7*	0.0	1.5*	0.3*
Extratropical SST	0.6*	0.3*	0.4	−0.1
Global SST and sea ice	0.9*	1.9*	2.3*	0.3*
JRA-55	−2.5	1.5	−5.7	−1.6

forced with different lower-boundary conditions. See Supplement 1 for the details of boundary conditions and definitions of responses to them. Each of the five experiments has 100 ensemble members integrated from 1 September 2020 through 31 January 2021. This ensemble size has been determined following Mori et al. (2014), who noted that the response to SIAs could not be detected with less than 80 ensemble members.

3. Results

3.1 Ensemble-mean responses to SIA and SSTA

In December 2020, a cold SAT anomaly (SATA) was observed in JRA-55 mainly over midlatitude Eurasia (Fig. 2a), while in January 2021, the cold anomaly region shifted to subpolar Eurasia (Fig. 2c). The SATs averaged over midlatitude Eurasia (35°N−50°N, 60°E−120°E) in December 2020 and over subpolar Eurasia (55°N−70°N, 60°E−120°E) in January 2021 were both the third lowest among the last 42 Decembers (1979−2020) and the last 42 Januarys (1980−2021), respectively. Meanwhile, warm SATAs were observed over the BKS in both months. The pair of this warm anomaly and the midlatitude cold anomaly in December are characteristic of the WACE pattern (Fig. 2a).

Figure 2b shows the 100-member ensemble-mean SAT response to the observed SIA in December 2020. A warm response is found over the Arctic Ocean including the BKS, while a significant cooling response is located over midlatitude Eurasia. The area-averaged SAT response over midlatitude Eurasia to the SIA is −0.4 K, which is statistically significant at the 5% level (Table 1), suggesting that a part of the observed cooling (−2.5 K in JRA-55) is attributable to this response to the SIA. In fact, the observed SIA may have doubled the occurrence probability of the observed cooling (see Supplement 2). The pair of the cooling response over midlatitude Eurasia and warming response over the BKS suggest that the SIA forced, at least partly, the WACE pattern in this month. In contrast, the response to the observed global SSTA features uniform warming over Eurasia (not shown). The area-averaged response to the global SSTA is positive in midlatitude Eurasia (+1.0 K; Table 1). Responses to tropical and extratropical SSTAs both contribute to this warming over Eurasia (Table 1). The response to the concurrent SSTA and SIA is similar to the response to the SSTA only, which suggests the relatively weak response to the SIA.

In the mid-troposphere (Fig. 3a), a positive height anomaly

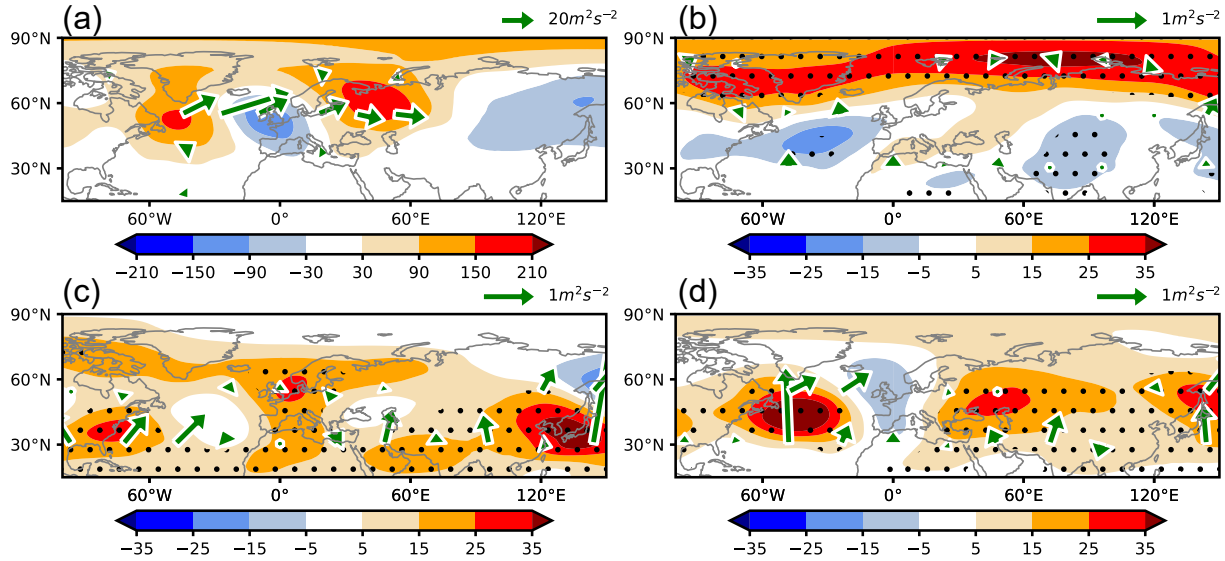

Fig. 3. (a) 500-hPa geopotential height anomaly in December 2020 based on JRA-55. The unit is m. Green arrows signify the wave-activity flux ($m^2\ s^{-2}$). (b) As in (a), but for AGCM-simulated 500-hPa geopotential height response to observed SIAs in December 2020. Dots represent anomalies significant at the 5% level with Student's *t*-test. (c) As in (b), but for the AGCM response to observed tropical SSTAs. (d) As in (b), but for the AGCM response to observed extratropical SSTAs.

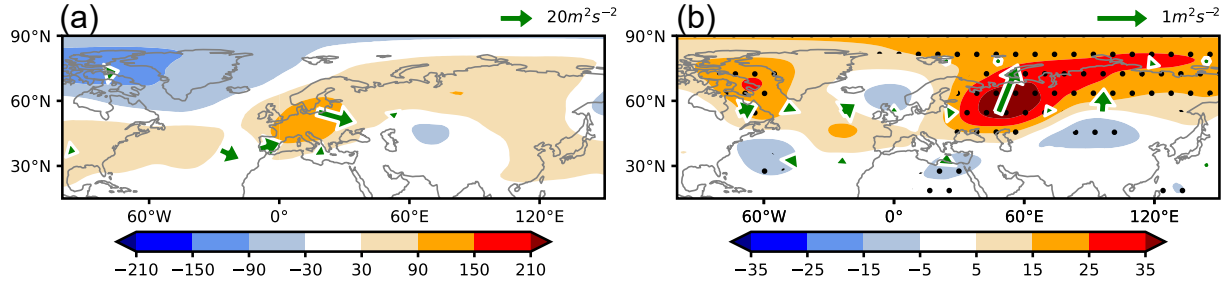

Fig. 4. As in Fig. 3a and b, but for November 2020.

was observed in December over the Ural Mountains (40°E−70°E) with a negative height anomaly over midlatitude Eurasia around 100ºE. These anomalies should induce low-level anomalous northerlies in between, contributing to the cold SATA (Fig. 2a). In addition, positive and negative height anomalies were observed over the North Atlantic and Europe, respectively, with eastward wave-activity flux (Takaya and Nakamura 2001), suggesting that Rossby wave propagation from the Atlantic may also contribute to the formation of the WACE anomalies (Fig. 3a). In the model response to the SIA, the positive height response over the Ural Mountains is not statistically significant (Fig. 3b). However, the height response over the Ural Mountains in November shows clear resemblance to the observed anomaly in December (Fig. 4b). This positive height response combined with the negative response downstream, both of which are statistically significant, should induce low-level northerlies and thus cooling in midlatitude Eurasia, which persists until December. Note that the corresponding positive height anomaly is not observed in November in JRA-55 (Fig. 4a). This disagreement may be related to a tendency that AFES responses to SIAs precede observed anomalies associated with the SIAs (Nakamura et al. 2015). The wave propagation from the Atlantic is missing in the response to the SIA. In contrast, as a response to the extratropical SSTA (Fig. 3d), prominent anticyclonic anomalies are simulated over the Ural Mountains and the midlatitude North Atlantic, although the Eurasian cooling is not simulated (figure not shown). The response to the tropical SSTA features no well-defined mid-tropospheric circulation anomalies over Eurasia except around Japan and Europe (Fig. 3c).

In January 2021, a cooling response to the observed SIA is found mainly over the southern portion of the Far East (Fig. 2d), and the observed cooling in subpolar Eurasia (Fig. 2c) is not simulated. Nor can SSTAs explain the cooling in subpolar Eurasia (Table 1). Rather, the tropical SSTA induces strong warming over subpolar Eurasia. In the mid-troposphere, the ridge over the Ural Mountains was also observed in JRA-55 as in December but with smaller amplitude and a slight southward shift (Fig. 5a). A negative height anomaly over Eurasia was also observed, but with a displacement to northeastern Eurasia. Those height anomalies may have forced the subpolar surface cooling (Fig. 2c). The AGCM height response to the observed SIA does not correspond to the observed anomalies (Fig. 5b). The responses to the tropical and extratropical SSTAs resemble those in December, but with larger amplitude (Figs. 5c and 5d). As the response to the extratropical SSTAs (Fig. 5d), a wave train, which consists of positive height responses over the North Atlantic and the Ural Mountains and a negative response over Europe, is more pronounced with the eastward wave-activity flux. The wave train over western Eurasia is like its observational counterpart, although the positive response over the North Atlantic does not correspond to the observed anomaly.

3.2 Leading modes of atmospheric variability

a. December 2020

Here, we discuss the relationship between the observed SATAs and the leading atmospheric modes. We applied an Empirical Orthogonal Function (EOF) analysis to interannual variability of

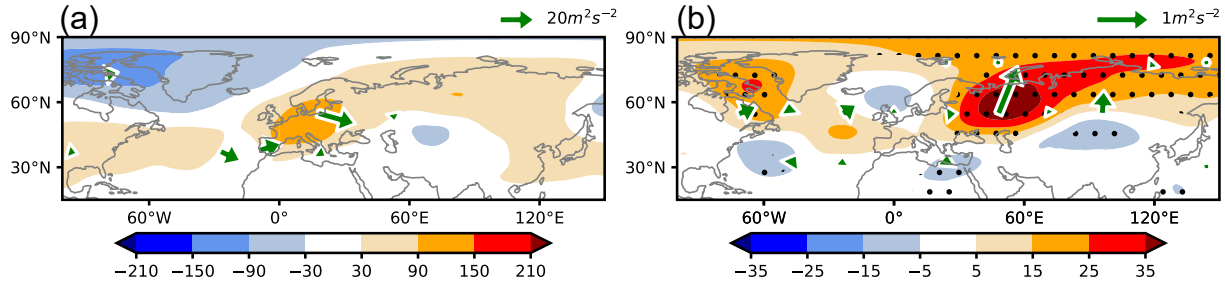

Fig. 5. As in Fig. 3, but for January 2021.

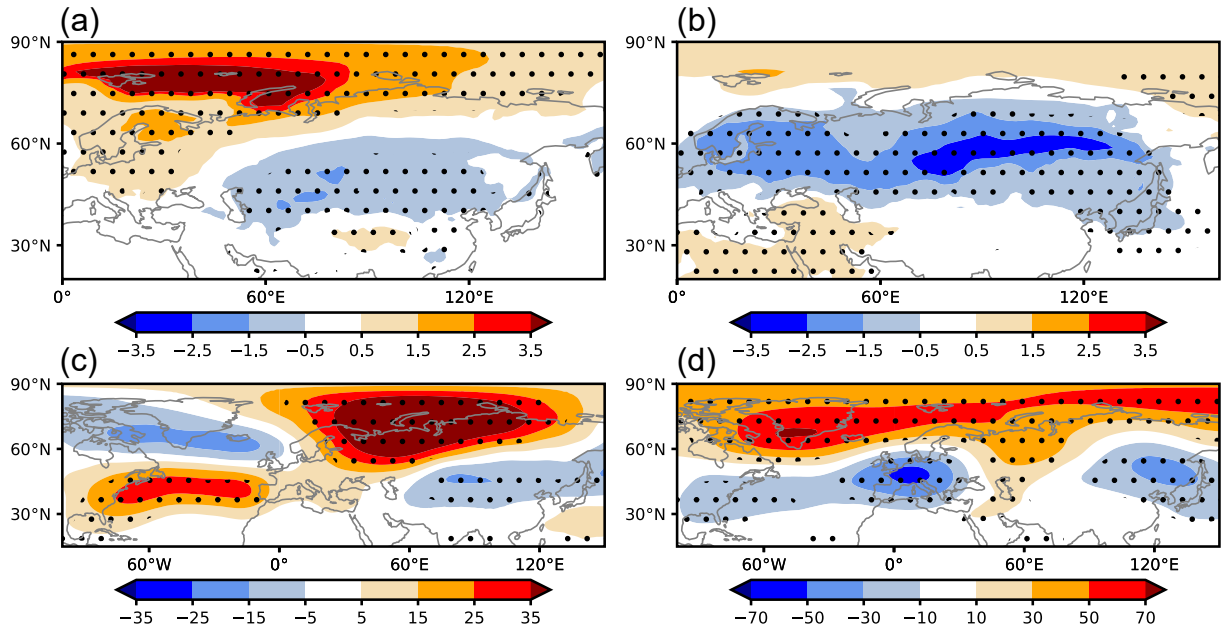

Fig. 6. (a) SATAs regressed onto the WACE index in December based on JRA-55. The unit is K. Dots represent correlation significant at the 5% level with Student's *t*-test. (b) As in (a), but for regression onto the sign-reversed AO index in January. (c) As in (a), but for 500-hPa geopotential height anomalies. The unit is m. (d) As in (b), but for 500-hPa geopotential height anomalies.

monthly-mean SAT fields of JRA-55. The analysis was conducted separately for December (1979−2020) and January (1980−2021). The EOF domain is set to Eurasia (20°N−90°N, 0°E−180°), following the definition of the WACE pattern by Mori et al. (2014). The second EOF of SAT fields in December, which explains 18.5% of the total variance, highlights the Arctic-midlatitude dipole structure (Fig. 6a) and can thus be regarded as the WACE pattern. Hereafter, the associated principal component (PC) time series is used as the observed WACE index. Similarity of the observed SATA pattern in December 2020 (Fig. 2a) to this WACE pattern is notable. In fact, the normalized WACE index in December 2020 is +1.5, which is the 5th highest during the analysis period. The 500-hPa height anomalies associated with the WACE pattern are characterized by an anticyclonic anomaly centered around the BKS and a weaker cyclonic anomaly to its southeast (Fig. 6c). The observed height anomalies in December 2020 (Fig. 3a) also project well onto this pattern.

The contributions of boundary forcing to the occurrence of the WACE pattern are evaluated by following Mori et al. (2014) and Nishii et al. (2020). The EOF analysis was applied to the combined 500-member ensemble (i.e., 100 ensemble members for each of the five experiments) of the SAT fields. The variability here includes both unforced atmospheric internal variability and variability modulated by lower-boundary forcings. Unlike JRA-55, it is the first EOF (contribution: 26.6%) whose associated SATA resembles the WACE pattern (not shown). We thus use the normalized first PC as the model WACE index. The associated height anomaly pattern also resembles that of JRA-55 (not shown). Note that the WACE pattern is essentially an internal atmospheric variability, and boundary conditions modulate its occurrence probability (Mori et al. 2014; see also Supplement 2). The response of the WACE index to the SIA in December is +1.7, which is statistically significant at the 5% level based on the Student's *t*-test (Table 1), suggesting that the SIA in December 2020 likely contributed to the occurrence of the WACE pattern. The impact of global SSTA on the WACE pattern is also estimated to be +0.4, which is also statistically significant, though smaller compared to the SIC influence. The response to the tropical SSTA is statistically insignificant, while the response to the extratropical SSTA is significant. These results suggest that it is the SSTA in the extratropics rather than that in the tropics that can contribute to the occurrence of the WACE pattern. In conclusion, both SIA and extratropical SSTA are likely to have contributed to the WACE pattern observed in December 2020 by modulating its occurrence probability.

b. January 2021

In January, the observed WACE index is smaller (+0.4), and the observed SATA does not feature the WACE pattern (Fig. 2c). We applied an EOF analysis to sea-level pressure (SLP) fields of JRA-55 over the extratropical Northern Hemisphere (20°N−90°N, 0°E−360°), as in Thompson and Wallace (1998). The first EOF

(contribution: 25.7%) should represent the AO, and the corresponding PC is used as the observed AO index. The AO index is −1.6 in January 2021. This is the third lowest during the analysis period, which means that the negative AO was dominant in January 2021. A cool SATA associated with the negative AO in January was located over subpolar Eurasia (Fig. 6b), while the 500-hPa height anomaly was characterized by a positive anomaly over the Arctic, a pressure ridge around 60°E, and cyclonic anomalies upstream and downstream of the ridge (Fig. 6d). (Note that the signs of anomalies are reversed in Figs. 6b and 6d to illustrate the negative AO). These SAT and height anomalies associated with the negative AO characterize the observed anomalies in January 2021 (Figs. 2c and 5a).

To evaluate the role of SIA and SSTA in forcing the observed negative AO, we applied an EOF analysis to the SLP fields of the 500 ensemble members of the AGCM experiments for January 2021. The SAT and 500-hPa height anomalies associated with the first EOF of the AGCM (contribution: 20.3%) well capture those of JRA-55 (not shown). This suggests that our AGCM reasonably simulates the variability associated with the AO. The first PC is thus considered as the model AO index.

The response to the SIA is small and insignificant (Table 1), which suggests that the SIC forcing is not effective in modulating the AO variability. The global SSTA influence on the AO pattern is significantly positive, mainly due to the tropical SSTA (Table 1). However, the observed phase of the AO is negative. Our analysis suggests that neither SIA nor SSTAs can explain the observed negative AO and the associated subpolar Eurasian cooling in January 2021.

4. Conclusions and discussion

We investigated the factors that potentially contributed to cooling observed over midlatitude Eurasia in December 2020 and over subpolar Eurasia in January 2021 based on AGCM experiments. The midlatitude cooling in December was associated with the WACE pattern, and the AGCM experiments suggest that it was likely forced, at least partly, by the SIA. The extratropical SSTA may make an additional contribution to the WACE pattern, though unlikely to account for the Eurasian cooling. The subpolar cooling in January was associated with the negative AO. Significant contribution to it from the SIA and SSTA was, however, not detected.

The cooling response to the SIA in December may be consistent with ZZD22, while inconsistent with previous studies who argues that the model response to the SIA is indiscernible (e.g., Ogawa et al. 2018; Komatsu et al. 2022). The reason for this discrepancy is unclear and will be our future work.

In addition, our results may be inconsistent with ZZD22 in that the response to the SIA in our experiments failed to simulate the stratospheric pathway (Nakamura et al. 2016) associated with warming in the polar stratosphere (not shown), which might trigger the negative AO. Thus, our experiment cannot exclude the possibility that the observed AO was forced by the SIA. The warm response to the extratropical SSTA, which should involve the PDO-related anomaly is observed in our results, which may also be inconsistent with them. Those inconsistencies are also our future work.

The cooling response in our AGCM (−0.4 K) is weaker than its observed cooling and small when compared with the standard deviation among ensemble members being 1.3 K. This may be consistent with the underestimated model response to the SIA in many AGCMs (Mori et al. 2019) and with Zhang22. Nevertheless, the observed WACE index in December 2020 (+1.5) corresponds to the 95th percentile of the WACE index distribution among the 100 ensemble members of the CLM-IC experiment. This means that a chance of the WACE occurrence in December 2020 is low if only atmospheric internal variability is considered, suggesting the importance of sea ice forcing.

Arctic SIAs in December and January are almost unchanged, but the latitudes of negative SAT responses over Eurasia shifted meridionally (Figs. 2b and 2d). The reason is, however, unclear and will be our future work.

Our AGCM response to the extratropical SSTA accompanies a wave train from the North Atlantic with a ridge over the Ural Mountains (Figs. 3d and 5d), which resembles the observed height anomalies (Figs. 3a and 5a). This wave train and a warm SSTA over the North Atlantic (Fig. 1a) may be consistent with Sato et al. (2014), who pointed out that a warm SSTA over the North Atlantic can force a wave train downstream. They also argue that the wave train leads to cooling over Eurasia. However, our AGCM experiments are unable to simulate such cooling as a response to the extratropical SSTA, but they simulate warming instead (Table 1). Further analysis is needed to evaluate the relationship between SSTAs and the Eurasian cooling.

Acknowledgements

This study is supported in part by the Arctic Challenge for Sustainability II (ArCS II), Program Grant Number JPMXD 1420318865 and by the Japanese Ministry of Environment through the Environment Research and Technology Development Fund 2-1904 (JPMEERF20192004). This work is also supported by the Japan Society for the Promotion of Science (JSPS) through a Grant-in-Aid for Scientific Research in Innovative Area 6102 (KAKENHI Grant No. 19H05701, JP19H05702, and JP19H05703) and through KAKENHI Grants JP18H01278, JP19H01377, JP19H 01964, JP20H01970, and JP22H01299 and by the Japan Science and Technology Agency through COI-NEXT JPMJPF2013. The JRA-55 reanalysis dataset is provided through the JMA Data Consortium, and the NOAA OISST are provided by the NOAA-CIRES Climate Diagnostics Center, Boulder, Colorado, from their website (http://www.cdc.noaa.gov/). The Earth Simulator was utilized in support of JAMSTEC.

Edited by: M. Niwano

Supplements

Supplement 1: Details of boundary conditions and definitions of responses.

Supplement 2: Modulation of probability of extreme cooling and the WACE pattern.

References

Bueh, C., J. Peng, D. Lin, and B. Chen, 2022: On the two successive supercold waves straddling the end of 2020 and the beginning of 2021. *Adv. Atmos. Sci.*, **39**, 591−608.

Huang, B., C. Liu, V. Banzon, E. Freeman, G. Graham, B. Hankins, T. Smith, and H.-M. Zhang, 2021: Improvements of the Daily Optimum Interpolation Sea Surface Temperature (DOISST) Version 2.1. *J. Climate*, **34**, 2923−2939.

Inoue, J., M. E. Hori, and K. Takaya, 2012: The role of Barents Sea ice in the wintertime cyclone track and emergence of a warm-Arctic cold-Siberian anomaly. *J. Climate*, **25**, 2561−2568.

Kobayashi, S., Y. Ota, Y. Harada, A. Ebita, M. Moriya, H. Onoda, K. Onogi, H. Kamahori, C. Kobayashi, H. Endo, K. Miyaoka, and K. Takahashi, 2015: The JRA-55 reanalysis: General specifications and basic characteristics. *J. Meteor. Soc. Japan*, **93**, 5−48.

Komatsu, K., Y. Takaya, and T. Toyoda, 2022: Response of Eurasian temperature to Barents–Kara Sea ice: Evaluation by multi-model seasonal predictions. *Geophys. Res. Lett.*, **49**, e2021GL097203.

Kuwano-Yoshida, A., T. Enomoto, and W. Ohfuchi, 2010: An improved PDF cloud scheme for climate simulations. *Quart. J. Roy. Meteor. Soc.*, **136**, 1583−1597.

Mori, M., M. Watanabe. H. Shiogama, J. Inoue, and M. Kimoto, 2014: Robust Arctic sea-ice influence on the frequent Eur-

asian cold winters in past decades. *Nature Geosci.*, **7**, 869−873.

Mori, M., Y. Kosaka, M. Watanabe, H. Nakamura, and M. Kimoto, 2019: A reconciled estimate of the influence of Arctic sea-ice loss on recent Eurasian cooling. *Nature Climatic Change*, **9**, 123−129.

Nakamura, T., K. Yamazaki, K. Iwamoto, M. Honda, Y. Miyoshi, Y, Ogawa, and J. Ukita, 2015: A negative phase shift of the winter AO/NAO due to the recent Arctic sea-ice reduction in late autumn. *J. Geophys. Res. Atmos.*, **120**, 3209−3227.

Nakamura, T., K. Yamazaki, K. Iwamoto, M. Honda, Y. Miyoshi, Y. Ogawa, Y. Tomikawa, and J. Ukita, 2016: The stratospheric pathway for Arctic impacts on midlatitude climate. *Geophys. Res. Lett.*, **43**, 3494−3501.

Nishii, K., B. Taguchi, and H. Nakamura, 2020: An atmospheric general circulation model assessment of oceanic impacts on extreme climatic events over Japan in July 2018. *J. Meteor. Soc. Japan*, **98**, 801−820.

Ogawa, F., N. Keenlyside, Y. Gao, T. Koenigk, S. Yang, L. Suo, T. Wang, G. Gastineau, T. Nakamura, H.-N. Cheung, N.-E. Omrani, J. Ukita, and V. Semenov, 2018: Evaluating impacts of recent Arctic sea-ice loss on the northern hemisphere winter climate change. *Geophys. Res. Lett.*, **45**, 3255−3263.

Ohfuchi, W., H. Nakamura, M. K. Yoshioka, T. Enomoto, K. Takaya, X. Peng, S. Yamane, T. Nishimura, Y. Kurihara, and K. Ninomiya, 2004: 10-km mesh meso-scale resolving simulations of the global atmosphere on the Earth Simulator: Preliminary outcomes of AFES (AGCM for the Earth Simulator). *J. Earth Simulator*, **1**, 8−34.

Overland, J. E., T. J. Ballinger, J. Cohen, J. A. Francis, E. Hanna, R. Jaiser, B.-M. Kim, S.-J. Kim, J. Ukita, T. Vihma, M. Wang, and X. Zhang, 2021: How do intermittency and simultaneous processes obfuscate the Arctic influence on midlatitude winter extreme weather events? *Environ. Res. Lett.*, **16**, 043002.

Reynolds, R. W., T. M. Smith, C. Liu, D. B. Chelton, K. S. Casey, and M. G. Schlax, 2007: Daily high-resolution-blended analyses for sea surface temperature. *J. Climate*, **20**, 5473−5496.

Sato, K., J. Inoue, and M. Watanabe, 2014: Influence of the Gulf Stream on the Barents Sea ice retreat and Eurasian coldness during early winter. *Environ. Res. Lett.*, **9**, 1748−9326.

Takaya, K., and H. Nakamura, 2001: A formulation of a phase-independent wave-activity flux for stationary and migratory quasigeostrophic eddies on a zonally varying basic flow. *J. Atmos. Sci.*, **58**, 608−627.

Thompson, D. W. J., and J. M. Wallace, 1998: The Arctic oscillation signature in the wintertime geopotential height and temperature fields. *Geophys. Res. Lett.*, **25**, 1297−1300.

Tyrlis, E., E. Manzini, J. Bader, J., Ukita, H. Nakamura, and D. Matei, 2019: Ural blocking driving extreme Arctic sea ice loss, cold Eurasia, and stratospheric vortex weakening in autumn and early winter 2016−2017. *J. Geophys. Res. Atmos.*, **124**, 11313−11329.

Yao, Y., W. Q. Zhang, D. H. Luo, L. H. Zhong, and L. Pei, 2022: Seasonal cumulative effect of Ural blocking episodes on the frequent cold events in China during the early winter of 2020/21. *Adv. Atmos. Sci.*, **39**, 609−624.

Zhang, R., R. Zhang, and G. Dai, 2022: Intraseasonal contributions of Arctic sea-ice loss and Pacific decadal oscillation to a century cold event during early 2020/21 winter. *Climate Dyn.*, **58**. 741−758.

Zhang, X. D., Y. F. Fu, Z. Han, J. E. Overland, A. Rinke, H. Tang, T. Vihma, and M. Y. Wang, 2022: Extreme cold events from East Asia to North America in winter 2020/21: Comparisons, causes, and future implications. *Adv. Atmos. Sci.*, **39**, 553−565.

Zheng, F., Y. Yuan, Y. Ding, K. Li, X. Fang, Y. Zhao, Y. Sun, J. Zhu, Z. Ke, J. Wang, and X. Jia, 2022: The 2020/21 extremely cold winter in China influenced by the synergistic effect of La Niña and warm Arctic. *Adv. Atmos. Sci.*, **39**, 546−552.

Manuscript received 4 April 2022, accepted 19 July 2022
SOLA: *https://www.jstage.jst.go.jp/browse/sola/*